

# Tumor volume delineation: A pilot study comparing a digital positron-emission tomography prototype with an analog positron-emission tomography system

## ABSTRACT

We evaluated the potential differences of a digital positron-emission tomography (PET) prototype equipped with photon-counting detectors (D-PET, Philips Healthcare, Cleveland, Ohio, USA) in tumor volume delineation compared with the analog Gemini TF PET system (A-PET, Philips). Eleven oncologic patients first underwent clinical fluorodeoxyglucose (FDG) PET/computed tomography (CT) on A-PET. The D-PET ring was then inserted between the PET and CT scanner of A-PET and the patient was scanned for the second time. Two interpreters reviewed the two sets of PET/CT images for image quality and diagnostic confidence. FDG avid lesions were evaluated for volume measured at 35% and 50% of maximum standard uptake value (SUV) thresholds (35% SUV, 50% SUV), and for SUV gradient as a measure of lesion sharpness. Bland–Altman plots were used to assess the agreement between the two PET scans. Qualitative lesion conspicuity, sharpness, and diagnostic confidence were greater at D-PET than that of A-PET with favorable inter-rater agreements. Median lesion size of the 24 measured lesions was 1.6 cm. The lesion volume at D-PET was smaller at both 35% SUV and 50% SUV thresholds compared with that of A-PET, with a mean difference of 3680.0 mm<sup>3</sup> at 35% SUV and 835.3 mm<sup>3</sup> at 50% SUV. SUV gradient was greater at D-PET than at A-PET by 49.2% (95% confidence interval: 34.1%–60.8%). Given the smaller volume definition, coupled with improved conspicuity and sharpness, digital PET may be more robust and accurate in tumor rendering compared with analog PET not only for radiotherapy planning but also in prognostication and systemic treatment monitoring.

**Keywords:** Digital positron-emission tomography, direct photon counting, fluorodeoxyglucose positron-emission tomography, tumor volume rendering

## INTRODUCTION


Positron-emission tomography/computed tomography (PET/CT) is an established imaging modality in oncology for staging, restaging, and monitoring response to therapy. PET/CT with F-18 fluorodeoxyglucose (FDG) has become a routine examination for baseline staging and radiation treatment planning of non-small cell lung cancer.<sup>[1-4]</sup> One distinct advantage of PET-based volume rendering for radiotherapy planning is its potential to complement anatomical-based volume to improve tumor delineation, reducing intra- and inter-observer variability.<sup>[3]</sup> Careful optimizations of image characteristics and delineation methods are important to obtain accurate and reproducible volume-based PET parameters.

Steady improvements in PET detector design and architecture, as well as the implementation of time-of-flight (TOF) technology, have resulted in significant improvements in PET image quality.<sup>[5]</sup> A new scintillation detector – digital photon

**NGHI C. NGUYEN, JOSE VERCHER-CONEJERO<sup>1</sup>, PETER FAULHABER<sup>1</sup>**

Department of Radiology, University of Pittsburgh, Pittsburgh, PA 15213, <sup>1</sup>Department of Radiology, Case Western Reserve University, University Hospitals Case Medical Center, Cleveland, OH, USA

**Address for correspondence:** Dr. Nghi C. Nguyen, Department of Radiology, UPMC Presbyterian, 200 Lothrop Street East Wing, Suite 200, Pittsburgh, PA 15213, USA.  
E-mail: nncc.nguyen@gmail.com

Access this article online	
<b>Website:</b> www.wjnm.org	<b>Quick Response Code</b> 
<b>DOI:</b> 10.4103/wjnm.WJNM_22_18	

This is an open access journal, and articles are distributed under the terms of the Creative Commons Attribution-NonCommercial-ShareAlike 4.0 License, which allows others to remix, tweak, and build upon the work non-commercially, as long as appropriate credit is given and the new creations are licensed under the identical terms.

**For reprints contact:** reprints@medknow.com

**How to cite this article:** Nguyen NC, Vercher-Conejero J, Faulhaber P. Tumor volume delineation: A pilot study comparing a digital positron-emission tomography prototype with an analog positron-emission tomography system. World J Nucl Med 2019;18:45-51.

counters – was recently introduced by Philips Healthcare, with which conventional photomultipliers have been replaced with high-performance digital detectors and single-photon avalanche photodiodes, enabling true digital photon counting.<sup>[6-8]</sup> In addition to digital photon counting, the detector element size is matched with 4 mm × 4 mm lutetium yttrium orthosilicate crystal (LYSO), enabling a 1:1 coupling of signals, which eliminates the need for Anger logic for crystal identification. A PET prototype equipped with digital photon counters and TOF technology (D-PET, Philips Healthcare) was installed at the Department of Radiology, University Hospitals Case Medical Center, Cleveland, Ohio, in 2012 as part of an industry-sponsored clinical trial. The current pilot study aims to assess the potential differences as well as benefits of D-PET in tumor volume definition compared with an analog Gemini TF PET/CT system, Philips Healthcare (A-PET).

## MATERIALS AND METHODS

### Patient population

This prospective study includes patients aged 18 years or older who were referred for a clinical PET/CT examination. From a pool of oncologic patients undergoing clinical FDG PET/CT for initial diagnosis and staging as well as restaging, 23 consecutive patients were enrolled in this study. Of these, three patients were excluded from the analysis because only limited imaging of the pelvis was available; thus, twenty patients were included for image review. The study was approved by the Institutional Review Board, and all patients signed a written consent form.

### Imaging protocol

All patients underwent a single-injection, dual-imaging protocol including the clinical PET/CT scan on the Gemini TF PET/CT (A-PET) and subsequent research PET scanning (D-PET). For this research, we took advantage of the A-PET feature that allows the PET gantry to be separated from the CT gantry by approximately 3 ft. After completion of the clinical PET/CT scan on the A-PET, the examination table was withdrawn, and the patient was asked to remain still on the table. The D-PET ring was inserted in the gap between the PET and CT gantry of the A-PET scanner. Subsequently, the patients underwent an additional acquisition with D-PET using the same axial field of view (FOV) as A-PET. The same CT data of the clinical PET/CT were used for attenuation correction and anatomic correlation with D-PET images. As a result, there was no additional radiation other than that already incurred during the clinical PET/CT examination.

### Clinical positron-emission tomography/computed tomography scanning

Patients fasted for at least 4 h before the examination. The CT consisted of a 16-slice multidetector helical CT and was obtained

before the PET scan. The CT data were used for generation of the CT transmission map, image fusion, and anatomic correlation with the PET findings (A-PET and D-PET). The parameters for the CT were based on institutional guidelines: 120 kVp, pitch of 0.829, and 100 mAs (patient weight <68 kg) or 150 mAs (patient weight ≥68 kg). No oral or intravenous contrast was administered. The PET scanner has an active transverse FOV of 57.6 cm. For PET scanning, the matrix size was 144 mm × 144 mm; the voxel size was 4 mm × 4 mm × 4 mm. The scan time per bed position was as follows: 1.5 min/bed, patient weight 45.4–68.0 kg; 2.0 min/bed, patient weight 68.1–90.7 kg; 2.5 min/bed, patient weight 90.8–136.1 kg; and 3.0 min/bed, patient weight >136.1 kg. A list-mode TOF algorithm and line-of-response row-action maximum-likelihood algorithm method, the so-called BLOB-OS-TF, was used for image reconstruction.<sup>[9,10]</sup>

### Research positron-emission tomography scanning

The D-PET prototype was an investigational device as defined by 21 Code of Federal Regulations Part 812. As a research device, it was not commercially available and did not have Food and Drug Administration 510(k) clearance. After the completion of the clinical scan, the scanner table was then withdrawn, the D-PET ring was inserted between the PET scanner and CT scanner of the A-PET, and the patient was scanned for the second time and adjusted for tracer delay, using the same CT scan from A-PET for attenuation correction. D-PET has the same transverse FOV of 57.6 cm but a shorter axial FOV than the A-PET scanner (16.4 vs. 18.0 cm). However, the total scanning time was the same for both scanners after adjustment of tracer decay. Both A-PET and D-PET contain the same LYSO crystal material with 4 mm × 4 mm × 22 mm dimension. As with A-PET, the image reconstruction with 4-mm voxels and matrix size 144 mm × 144 mm, as well as the list-mode TOF with BLOB-OS-TF, was used for D-PET, but individual reconstruction parameters were kept as recommended by the manufacturer for both A-PET and D-PET to achieve optimal image characteristics. Point-spread function correction was not used for either system.

### Image review and data analyses

The images were reviewed and analyzed using the EBW workstation (version 4.5.3.40140; Philips Healthcare). Two experienced interpreters compared the two PET/CT datasets side by side for lesion conspicuity, sharpness, and diagnostic confidence using a 5-point scale (1, much worse; 2, worse; 3, same; 4, better; and 5, much better), all masked to the scanner type. The interpreters were, however, aware of the clinical indication for PET/CT.

One of the two interpreters obtained measurements of imaging data. The A-PET, D-PET, and CT images were opened

on the EBW workstation together, with PET/CT images being linked automatically. A maximum of six FDG avid lesions including the primary tumor, defined as those with maximum standard uptake value (SUV) greater than that of the liver parenchyma, were measured for each patient. Whenever possible, lesions from different body regions were preferred over those within the same region to allow for representative lesion measurements. The largest diameter of the lesions was measured on axial CT images. For volume delineation, thresholds at 35% and 50% of maximum SUV (35% SUV and 50% SUV) were used, which means that only tissue areas above these %SUV values are included for volume definition. The measure of lesion sharpness was defined as the greatest gradient in mean SUV between two adjacent pixels at the margin of an FDG-avid lesion.<sup>[11-14]</sup> The operator drew a straight line through the central area of the lesion to obtain the greatest SUV gradients at both margins of the lesion, and the averaged value (SUV gradient) was used for analysis.

**Statistical analysis**

Patient characteristics and visual evaluations were assessed using measures of central tendency (median, minimum–maximum, 95% confidence interval [CI]). For inter-rater agreement analyses, the original 5-point scores for lesion conspicuity, sharpness, and diagnostic confidence were re-assigned to 3-point scores (1 + 2 became 1; 3 became 2; and 4 + 5 became 3) considering the small sample size. Wilcoxon tests were used to compare lesion SUV threshold-based volumes as well as SUV gradients between the two PET systems. Besides linear correlations, Bland–Altman plots were used to assess the agreement of SUV threshold-based volumes between the two PET systems. *P* < 0.05 was considered statistically significant. The statistical software MedCalc 12.7.1 (MedCalc Software, Ostend, Belgium) was used.

**RESULTS**

Eleven of twenty patients were included in the final analyses because they showed FDG avid lesions greater than physiologic liver uptake. The median age of these 11 patients was 65 years (range, 47–81 years), of these 11 patients (3 women and 8 men), four underwent PET/CT scanning for staging (2 lung cancer, 1 breast cancer, and

1 tonsillar cancer) and seven for restaging (5 lung cancer, 1 lymphoma, and 2 malignant melanoma). The time delay between the two PET scans was 18 min (range, 7–55 min). Visual evaluations showed consistently greater image quality at D-PET than A-PET, with a median score of 4.0 (range, 4–5) for lesion conspicuity and sharpness each. Greater diagnostic confidence was also observed at D-PET with a median score of 4 (range, 3–5). The two readers showed excellent agreement for both lesion conspicuity and sharpness, with weighted kappa of 1.0 (95% CI, 1.0–1.0). The agreement was fair for diagnostic confidence with weighted kappa of 0.48 (95% CI, 0.05–0.91).

Median lesion size of the 24 measured lesions was 1.6 cm (range, 0.6–9.0 cm). The lesion volume at D-PET was smaller for both 35% SUV and 50% SUV with tighter CIs compared with that of A-PET [Table 1]. The percentage change in lesion volume was more drastic with 35% SUV than with 50% SUV (median –31.1%; 95% CI, –40.7% to –21.0% vs. median –19.1%; 95% CI –26.6% to –5.9%). For both 35% SUV and 50% SUV volumes, the correlation was excellent between the two PET scans [Table 1 and Figure 1]. Two examples of a metastatic cervical lymph node from tonsillar cancer and a lung primary are illustrated in Figures 2 and 3.

Bland–Altman analyses of 35% SUV data showed that, in 22 of the 24 lesions or one of the 11 patients, the D-PET volume was smaller by an average of –3680.0 mm<sup>3</sup> compared with that of A-PET. In two of the 24 lesions or two of the 11 patients, the 35% SUV volume at D-PET equaled to or was larger compared with that of A-PET [Figure 4]. At 50% SUV, in 19 of the 24 lesions or eight of the 11 patients, the D-PET volume was smaller by an average of –835.3 mm<sup>3</sup> compared with that of A-PET. In three of the 24 lesions or three of the 11 patients, the D-PET volume was larger compared with that of A-PET, and the volume was unchanged in one of the 24 patients.

SUV gradient was greater at D-PET than at A-PET, with excellent correlation between the two PET scanners [Table 1]. SUV gradient increased by 49.2% (95% CI, 34.1%–60.8%) with D-PET compared with A-PET. Correlation between percentage change in SUV gradient and percentage change in 35% SUV

**Table 1: Summary of standard uptake value threshold-based volume and standard uptake value gradient comparisons, *P*<0.05 for all parameters**

	Median (95% CI)		Correlation ( <i>r</i> )	Percentage difference median (95% CI)
	A-PET	D-PET		
35% SUV volume	6868 (3888-14,242)	5920 (2591-9493)	0.98	–31.1 (–40.7––21.0)
50% SUV volume	3840 (1888-7921)	3424 (1470-5154)	0.99	–19.1 (–26.6––5.9)
SUV gradient	2.7 (1.9-3.7)	4.6 (3.2-5.2)	0.90	49.2 (34.1-60.8)

PET: Positron-emission tomography; CI: Confidence interval; SUV: Standard uptake value

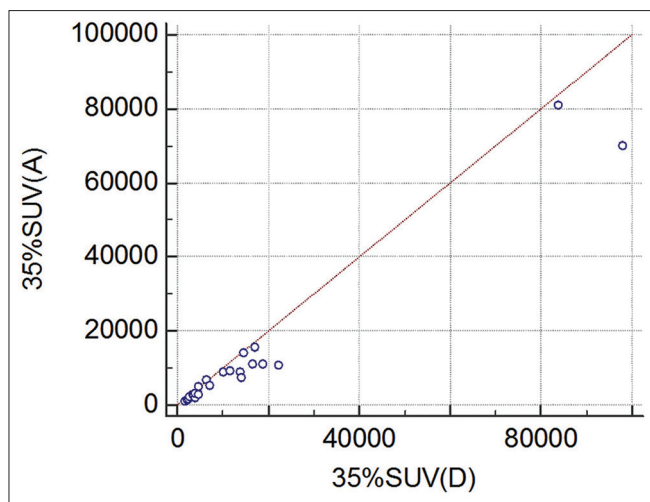


Figure 1: Correlation between A-positron emission tomography and D-positron emission tomography at 35% standard uptake value threshold

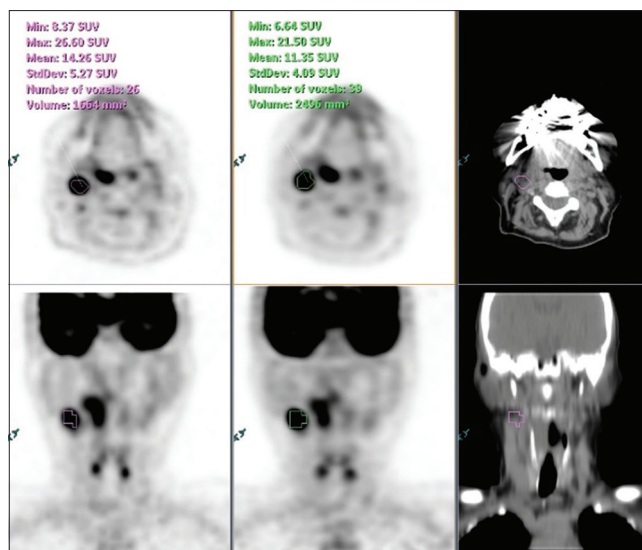


Figure 2: A 67-year-old woman with biopsy-proven squamous cell carcinoma of the right tonsil for staging. Axial and coronal A-positron emission tomography images (left) showed a volume of 2496 mm<sup>3</sup> at 35% standard uptake value threshold and D-positron emission tomography images (middle) showed a volume of 1664 mm<sup>3</sup> for the right Level II cervical lymph node, representing a -33.3% volume reduction at D-positron emission tomography; corresponding computed tomography images (right). Standard uptake value gradient was 8.3 at A-positron emission tomography and 11.1 at D-positron emission tomography, corresponding to a 33.7% increase in sharpness at D-positron emission tomography

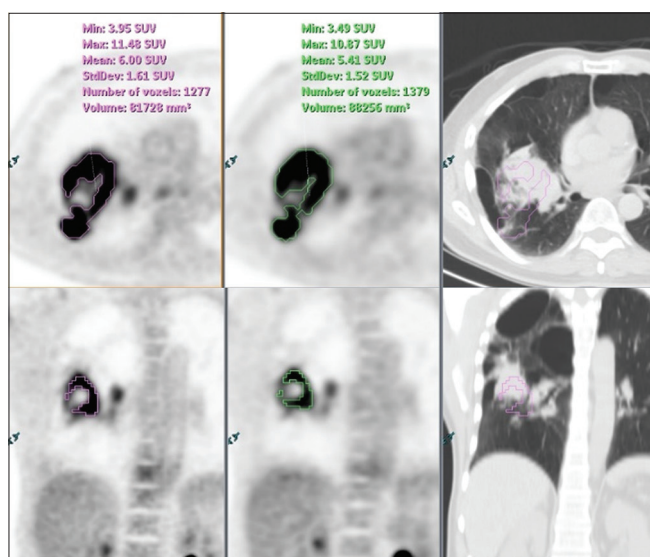


Figure 3: A 68-year-old man with a history of right lung small cell carcinoma for staging. Axial and coronal A-positron emission tomography images (left) showed a volume of 88,256 mm<sup>3</sup> at 35% standard uptake value threshold and D-positron emission tomography images (middle) showed a volume of 81,728 mm<sup>3</sup> for the right middle lobe primary, representing a -7.4% volume reduction at D-positron emission tomography; corresponding computed tomography images (right). Standard uptake value gradient was 3.8 at A-positron emission tomography and 4.0 at D-positron emission tomography, corresponding to a 5.0% increase in sharpness at D-positron emission tomography

volume as well as 50% SUV volume was fair ( $r = -0.49$  each,  $P = 0.01$ ).

## DISCUSSION

PET-based tumor definition such as metabolic tumor volume and total lesion glycolysis can play a significant role in prognostication and restaging and complement anatomical tumor definition for radiotherapy treatment planning.<sup>[1-4]</sup>

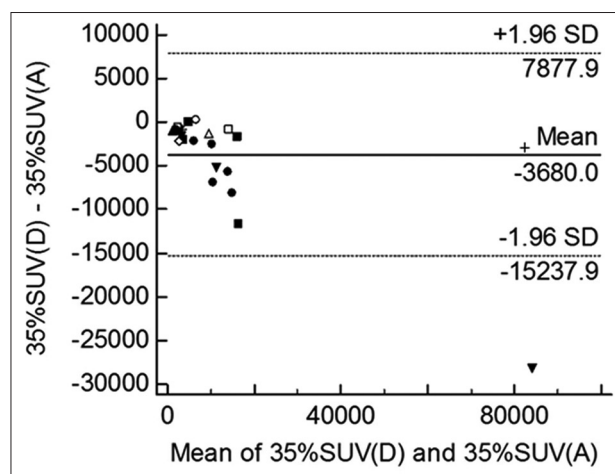


Figure 4: Bland-Altman plots of 35% standard uptake value threshold A-positron emission tomography (A) and D-positron emission tomography (D). Differences between A and D (Y-axis) are plotted against the averages of A and D. There was a systematic difference, in that D produced smaller volumes than A, with a mean difference of -3680.0 mm<sup>3</sup>

Accurate and robust methods are, however, required to achieve acceptable diagnostic and therapeutic implications. We present data about a digital PET prototype that was not approved by the Food and Drug Administration but had served for the clinical validation of the Vereos PET/CT (Philips Healthcare). This prototype scanner has performance characteristics similar to the commercially available Vereos PET/CT system, which provides excellent TOF-effective sensitivity (22.0 vs. >18.8)

and TOF localization (4.6 cm vs. 8.9 cm) compared with Gemini TF PET/CT system.<sup>[12,15]</sup> Hence, digital PET has the potential to optimize tumor quantification as well as volume rendering.

To our knowledge, this is the first study to assess the potential benefits of digital PET in tumor rendering. D-PET shows greater lesion conspicuity and sharpness compared with that of A-PET and is associated with favorable inter-rater agreements. Favorable measurements of SUV gradients further support the qualitative findings. Coupled with the increase in diagnostic confidence, the visual interpretation of tumor edge will improve as well as the intra- and inter-observer variability will decrease. The measurable increase in lesion sharpness with D-PET as well as its correlation with SUV threshold-based volumes, albeit fair with  $r = -0.49$ , is the result of improved detector design and image characteristics. Particularly, given the 1:1 coupling of signals and improved TOF resolution (495 ps A-PET; 307 ps D-PET), the spatial resolution with D-PET is improved, and a more uniform resolution can be achieved across the detector surface.<sup>[12]</sup> Although the reconstruction parameters were not the same and individually optimized for both PET systems, the image reconstruction algorithms, crystal material, and dimensions as well as matrix size were the same, and no point-spread function correction was used. Moreover, phantom studies facilitating a head-to-head comparison of the two PET systems at both clinical condition and high count statistics, using the same reconstruction algorithm and parameters, showed that despite lower NEMA (NU 2–2007) sensitivity, D-PET achieved greater contrast by as much as 12% and greater spatial resolution (6.55 mm vs. 6.90 mm full width at half maximum) compared with that of A-PET.<sup>[12]</sup> Therefore, the greater image quality observed with D-PET is not attributed to having a higher number of events, but rather the result of combined effects involving detector design, time digitizer, system corrections, and reconstruction parameters. The design of the digital PET prototype is, however, not without limitations. Although digital PET technology can provide improved performance and new features such as dark count rate suppression, the implementation of embedded readout circuitry into the detector chip by combining single-photon avalanche diodes (SPADs) with low-voltage complementary metal oxide-semiconductor logic on the same silicon substrate can face significant design constraints.<sup>[16,17]</sup> For example, placing the circuitry too close to the SPAD may decrease the fill factor, which may lead to suboptimal photon detection efficiency.<sup>[16,18]</sup> This effect might explain the lower NEMA sensitivity of the digital PET system compared with A-PET.<sup>[12]</sup> These technical challenges need to be resolved in future developments of digital PET systems.

Volume rendering based on SUV threshold method may not correlate well with SUV gradient method because the former is highly dependent on the scanner characteristics such as spatial resolution, reconstruction method, and filtering, which may affect the lesion maximum SUV and the lesion volume. The SUV gradient method is, however, less susceptible to changes in background SUV or maximum SUV because it is a function of relative voxel values at the lesion periphery.<sup>[14,19]</sup> D-PET shows smaller lesion volumes with tighter confidence intervals compared with A-PET at both 35% SUV and 50% SUV thresholds. Thus, digital PET has the potential to provide robust algorithms for reliable and precise tumor delineation.<sup>[20]</sup> Moreover, D-PET has the potential to reduce radiation dose as well as toxicity to the surrounding tissues. Areas of nonspecific uptake – such as atelectasis and physiologic liver uptake – may be better separated from the actual tumor because of higher contrast and sharpness. Hence, atelectasis may be better omitted during the radiation treatment planning. Another benefit of D-PET may involve radiation dose escalation, allowing accurate targeting of metabolically high-risk subvolumes within the tumor. Thresholds of 15%–50% of maximum SUV have been used for gross tumor volume delineation in radiotherapy planning.<sup>[2,21]</sup> Thus, the selected 35% SUV and 50% SUV thresholds are consistent with the range used in clinical practice and research.

Metabolic heterogeneity carries information about tumor aggressiveness and clinical outcome.<sup>[22]</sup> The clinical Vereos PET/CT scanner enables unrivaled 1-mm slice thickness reconstruction, which will enhance the detection and characterization of heterogeneity beyond the current analog PET systems.<sup>[8]</sup> Reconstruction with 1-mm slice thickness may be particularly helpful in radiotherapy planning of brain lesions when accurate tumor rendering is most vital to preserve normal brain tissue.

Our study has some limitations. Although the scan sequence, with D-PET being performed after A-PET in all patients, might favor D-PET regarding SUV measurements considering the gradual increase in tumor uptake, we did find a 36% increase in lesion maximum SUV from A-PET to D-PET (5.3 vs. 7.2), which however was not statistically significantly associated with the time delay. A recent study confirmed the greater image quality of the commercial digital PET system (Vereos PET/CT) compared to the analog Gemini TF system, in which the scan sequence varied among patients, and the digital PET scanning was performed either before or after the standard-of-care PET scan.<sup>[23]</sup>

We also acknowledge the small sample size of the pilot study, which may be associated with greater variations in the measurements. However, statistical tests account for the variability of the measurements and do not invalidate

a statistically significant difference. We did not include CT volumes to correlate with PET-based volumes because the goal was to demonstrate the potential differences between the two PET scanners and because the CT was noncontrast and would have limited the CT measurement in some lesions. Correlation of anatomical with metabolic volume, however, will be important in future studies. Only lesions with FDG uptake greater than that of the liver parenchyma were included so as to avoid automatic contouring of physiologic structures such as liver activity, but lesion contouring using the liver parenchymal uptake as a threshold is common in clinical practice.<sup>[1]</sup> The measured lesions were rather small with a median of 2.6 cm. It is likely that the volume reduction with D-PET is greater for smaller lesions than for larger ones because of the surface area–volume relationship. Consequently, the benefits of digital PET in tumor rendering may be less suitable for large lesions, but this needs to be evaluated in future clinical trials. We used the SUV threshold-based method for volume rendering to compare the two PET systems although the incorporation of other methods such as the SUV gradient-based method would have shed more light on the potential benefits of digital PET.

## CONCLUSIONS

Given the smaller volume definition, coupled with improved lesion conspicuity and sharpness, digital PET may be more robust and accurate in tumor rendering compared with analog PET, not only for radiotherapy planning but also in prognostication and systemic treatment monitoring. Digital PET opens new perspectives for tumor quantification and characterization but requires further validation in future clinical studies.

## Declaration of patient consent

The authors certify that they have obtained all appropriate patient consent forms. In the form the patient(s) has/have given his/her/their consent for his/her/their images and other clinical information to be reported in the journal. The patients understand that their names and initials will not be published and due efforts will be made to conceal their identity, but anonymity cannot be guaranteed.

## Financial support and sponsorship

Nil.

## Conflicts of interest

There are no conflicts of interest.

## REFERENCES

- Gill BS, Pai SS, McKenzie S, Beriwal S. Utility of PET for radiotherapy treatment planning. *PET Clin* 2015;10:541-54.
- Biehl KJ, Kong FM, Dehdashti F, Jin JY, Mutic S, El Naqa I, *et al.* 18F-FDG PET definition of gross tumor volume for radiotherapy of non-small cell lung cancer: Is a single standardized uptake value threshold approach appropriate? *J Nucl Med* 2006;47:1808-12.
- Price PM, Green MM. Positron emission tomography imaging approaches for external beam radiation therapies: Current status and future developments. *Br J Radiol* 2011;84:S19-34.
- Carlier T, Bailly C. State-of-the-art and recent advances in quantification for therapeutic follow-up in oncology using PET. *Front Med (Lausanne)* 2015;2:18.
- Surti S, Kuhn A, Werner ME, Perkins AE, Kolthammer J, Karp JS, *et al.* Performance of Philips Gemini TF PET/CT scanner with special consideration for its time-of-flight imaging capabilities. *J Nucl Med* 2007;48:471-80.
- Degenhardt C, Prescher G, Frach T, Thon A, de Gruyter R, Schmitz A, *et al.* The digital silicon photomultiplier – A novel sensor for the detection of scintillation light. *IEEE Nuclear Science Conference Record*; 2009. p. 2383-6.
- Degenhardt C, Rodrigues P, Trindade A, Zwaans B, Mulhens O, Dorscheid R, *et al.* Performance evaluation of a prototype positron emission tomography scanner using digital photon counters (DPC). *IEEE Nuclear Science Conference Record*; 2012. p. 2820-4.
- Adler S, Seidel J, Choyke P, Knopp MV, Binzel K, Zhang J, *et al.* Minimum lesion detectability as a measure of PET system performance. *EJNMMI Phys* 2017;4:13.
- Browne J, de Pierro AB. A row-action alternative to the EM algorithm for maximizing likelihood in emission tomography. *IEEE Trans Med Imaging* 1996;15:687-99.
- Surti S, Scheuermann J, El Fakhri G, Daube-Witherspoon ME, Lim R, Abi-Hatem N, *et al.* Impact of time-of-flight PET on whole-body oncologic studies: A human observer lesion detection and localization study. *J Nucl Med* 2011;52:712-9.
- Geets X, Lee JA, Bol A, Lonnew M, Grégoire V. A gradient-based method for segmenting FDG-PET images: Methodology and validation. *Eur J Nucl Med Mol Imaging* 2007;34:1427-38.
- Nguyen NC, Vercher-Conejero JL, Sattar A, Miller MA, Maniawski PJ, Jordan DW, *et al.* Image quality and diagnostic performance of a digital PET prototype in patients with oncologic diseases: Initial experience and comparison with analog PET. *J Nucl Med* 2015;56:1378-85.
- Wanet M, Lee JA, Weynand B, De Bast M, Poncelet A, Lacroix V, *et al.* Gradient-based delineation of the primary GTV on FDG-PET in non-small cell lung cancer: A comparison with threshold-based approaches, CT and surgical specimens. *Radiother Oncol* 2011;98:117-25.
- Werner-Wasik M, Nelson AD, Choi W, Arai Y, Faulhaber PF, Kang P, *et al.* What is the best way to contour lung tumors on PET scans? Multiobserver validation of a gradient-based method using a NSCLC digital PET phantom. *Int J Radiat Oncol Biol Phys* 2012;82:1164-71.
- Slomka PJ, Pan T, Berman DS, Germano G. Advances in SPECT and PET hardware. *Prog Cardiovasc Dis* 2015;57:566-78.
- Kang J, Choi Y. Simulation study of PET detector configuration with thick light guide and GAPD array having large-area microcells for high effective quantum efficiency. *Comput Methods Programs Biomed* 2016;131:79-87.
- Kolb A, Lorenz E, Judenhofer MS, Renker D, Lankes K, Pichler BJ, *et al.* Evaluation of geiger-mode APDs for PET block detector designs. *Phys Med Biol* 2010;55:1815-32.
- Rochas AP, Besse PA, Pantic D, Prijic Z, Popovic RS. Low-noise silicon avalanche photodiodes fabricated in conventional CMOS technologies. *IEEE Trans Electron Devices* 2002;49:387-94.
- Daisne JF, Sibomana M, Bol A, Doumont T, Lonnew M, Grégoire V, *et al.* Tri-dimensional automatic segmentation of PET volumes based on measured source-to-background ratios: Influence of reconstruction algorithms. *Radiother Oncol* 2003;69:247-50.
- Surti S. Update on time-of-flight PET imaging. *J Nucl Med* 2015;56:98-105.

21. Moon SH, Hyun SH, Choi JY. Prognostic significance of volume-based PET parameters in cancer patients. *Korean J Radiol* 2013;14:1-2.
22. Tixier F, Le Rest CC, Hatt M, Albarghach N, Pradier O, Metges JP, *et al.* Intratumor heterogeneity characterized by textural features on baseline 18F-FDG PET images predicts response to concomitant radiochemotherapy in esophageal cancer. *J Nucl Med* 2011;52:369-78.
23. Zhang JW, Bhatia P, Binzel K, Bai C, Maniawski P, Knopp M. Advantage and clinical benefit of 325ps TOF PET for lesion detectability. *J Nuclear Med* 2017;58 Suppl 1:1325.